INTERNATIONAL JOURNAL OF NUMERICAL METHODS IN FLUIDS, VOL. 13, 599–624 (1991)

A COMPRESSIBLE THREE-DIMENSIONAL DESIGN METHOD FOR RADIAL AND MIXED FLOW TURBOMACHINERY BLADES

M. ZANGENEH

Mechanical Engineering Department, University College London, Torrington Place, London WC1E 7JE, U.K.

SUMMARY

A fully three-dimensional compressible inverse design method for the design of radial and mixed flow turbomachines is described. In this method the distribution of the circumferentially averaged swirl velocity $r\bar{V}_\theta$ on the meridional geometry of the impeller is prescribed and the corresponding blade shape is computed iteratively. Two approaches are presented for solving the compressible flow problem. In the approximate approach the pitchwise variation in density is neglected and as a result the algorithm is simple and efficient. In the exact approach the velocities and density are computed throughout the three-dimensional flow field by employing a fast fourier transform in the tangential direction. The results of the approximate and exact approach are compared for the case of a high-speed (subsonic) radial-inflow turbine and it is shown that the difference between the blade shapes computed by the two methods is well within the manufacturing tolerances. The method was validated by calculating the flow through a designed high-speed radial-inflow turbine by using a three-dimensional inviscid Euler solver. Very good correlation was obtained between the specified and computed $r\bar{V}_\theta$-distributions.

KEY WORDS Radial turbomachinery Inverse design Potential flow

1. INTRODUCTION

There are two main approaches to the problem of aerodynamic design of turbomachinery blades, the direct and the inverse approach. In the direct approach the flow is computed for a given blade geometry, while in the inverse approach the required flow distribution is specified and the corresponding blade geometry is computed.

In recent years, as a result of development in computational fluid dynamics, considerable progress has been made in the numerical solution of the direct problem of turbomachinery design. For example, Denton[1] has numerically solved the three-dimensional Euler equations of motion and Dawes[2] and Hah *et al.*[3] have solved the 3D Navier–Stokes equations. Such methods are of substantial value to the designer, who can use them to analyse the flow conditions along vanes and blades. Ideally, it should then be possible to modify the blade shape if the flow conditions are not those required. In practice, however, there are difficulties in determining the degree and direction of any modifications, which difficulties are compounded by the fact that a change of blade shape at any location affects the flow at other parts of the blade. This is particularly so in the case of radial turbomachinery, where the blade geometry and the flow field are complicated and three-dimensional. As a result, the most rational approach for designing radial turbomachinery blades is to use a three-dimensional inverse design method.

0271–2091/91/150599–26$13.00

Received August 1990
Revised November 1990

A large number of inverse design methods are available in two dimensions and are widely used in the design of axial turbomachinery blades (e.g. References 4–7). Ideally one would like to prescribe the pressure or velocity distribution on the pressure and suction surfaces so that the blades are designed with optimized boundary layers (e.g. References 4 and 7). However, this type of design specification has no control over blade thickness and could result in an ill-posed problem. For example, Lighthill[4] found that it is impossible to specify the velocity distribution on the pressure and suction surfaces together with the upstream and downstream boundary conditions. As a result some authors prefer to prescribe the velocity (or pressure) distribution on the suction surface and the thickness distribution (e.g. Reference 5), whereas others have proposed methods in which the blade pressure loading is prescribed together with a thickness distribution (e.g. Reference 8).

In three dimensions, additional constraints on the choice of the design specification are required in order to avoid ill-posed problems. For instance, the value of the pressure along the hub of a radial turbomachinery vane is affected by the pressure along the shroud and as a result it is not possible to specify the pressure on the hub and shroud independently. The main implication of this fact is that very few three-dimensional inverse design methods are available at present. To the author's knowledge only five three-dimensional inverse design methods have been reported in the literature.[9–14] In all these methods either the blade loading or the circulation distribution is prescribed together with a thickness distribution. However, all these methods are affected by shortcomings which limit their application to problems of practical interest. The method of Zhao *et al.*[9] is limited to high-solidity blades, while the methods of Ockuroumu and McCune[10] and Falcao[11] are limited to the design of annular cascades of infinitely thin blades with constant hub and tip radius and small camber in incompressible flow. Although the methods of Tan *et al.*,[12] Borges[13] and Ghaly and Tan[14] can cope with highly loaded blades, they are also limited to incompressible flow.

This paper is concerned with the development of a three-dimensional inverse design method applicable to radial and mixed flow machines in subsonic compressible flow. The method is an extension of Hawthorne *et al.*'s[15] approach to the design problem in which the blades are represented by sheets of vorticity whose strength is determined by a specified distribution of circumferentially averaged swirl velocity $r\bar{V}_\theta$ (directly related to the bound circulation $2\pi r\bar{V}_\theta$) defined as

$$r\bar{V}_\theta = \frac{B}{2\pi}\int_0^{2\pi/B} rV_\theta \, d\theta,$$

where B is the number of blades. In this way it is possible to find an expression for the bound vorticity in terms of $r\bar{V}_\theta$ and the blade shape. From the vorticity it is then possible to calculate the velocity field, which is decomposed into circumferentially averaged and periodic components, by using the Clebsch formulation of steady rotational flow. The blade shape is determined by imposing the inviscid slip condition (i.e. blade shape aligned with the local velocity vector). Since the vorticity depends on the blade shape and the blade shape depends on the velocity field, the problem is solved iteratively. This method not only computes the blade shape but can also provide detailed information about the flow distribution (i.e. velocity, pressure, etc.) through the designed blade-row.

The original application of the method was confined to the design of 2D cascades of infinitely thin blades in incompressible flow. The method has since been extended to the three-dimensional design of axial machines by Tan *et al.*[12] and applied to the case of arbitrary meridional geometry by Borges[13] using the finite difference approach and by Ghaly and Tan[14] using the finite element approach.

This paper describes how the calculation for compressible flow can be performed by computing velocities and density throughout the 3D flow field. A second, approximate, approach to solve the compressible flow problem is also presented. In this approach the variation of density in the pitchwise direction is neglected and an approximate form of the continuity equation is used. In both approaches the partial differential equations modelling the flow field and the blade boundary condition are solved numerically by a using finite difference method on a body-fitted curvilinear computational plane.

2. DESCRIPTION OF THE METHOD

In the theory which will be presented in this paper the following assumptions will be made.

(a) The flow is steady, inviscid and uniform at the inlet, so that the only vorticity is the bound vorticity on the blades (Kelvin's theorem). Therefore we may express the vorticity in terms of a periodic delta function as[15,16]

$$\boldsymbol{\Omega} = \nabla \times \mathbf{V} = (\nabla r \bar{V}_\theta \times \nabla \alpha)\, \delta_p(\alpha), \tag{1}$$

where

$$\alpha = \theta - f(r, z) = n\frac{2\pi}{B} \tag{2}$$

represents the blade surfaces, θ is the tangential co-ordinate of a cylindrical–polar co-ordinate system and $f(r, z)$ is the angular co-ordinate of the point on the thin blade surface, or the so-called wrap angle. $\delta_p(\alpha)$ is the periodic delta function given by[17]

$$\delta_p(\alpha) = \frac{2\pi}{B} \sum_{n=-\infty}^{\infty} \delta\left(\alpha - n\frac{2\pi}{B}\right) = \mathrm{Re} \sum_{n=-\infty}^{\infty} e^{inB\alpha}. \tag{3}$$

The tangential mean of the delta function, $\delta_p(\alpha)$, is unity and hence the mean vorticity is given by

$$\bar{\boldsymbol{\Omega}} = \nabla \times \bar{\mathbf{V}} = (\nabla r \bar{V}_\theta \times \nabla \alpha). \tag{4}$$

(b) There is no trailing shed vorticity.
(c) The blades have zero thickness, so that they can be represented by a single sheet of vorticity. However, the blade blockage effects are accounted for by using a mean stream surface thickness parameter in the continuity equation of the mean flow.
(d) The working fluid is a perfect gas and the flow is subsonic.

2.1. Calculation of flow field—approximate approach

In this subsection we shall derive the governing equations of the mean and periodic flow based on the assumption that the pitchwise variation in density is negligible. For this purpose let us consider the continuity equation in steady flow in the relative frame of reference,

$$\nabla \cdot \rho \mathbf{W} = 0. \tag{5}$$

Since the flow field is to be solved by decomposing it into circumferentially averaged and periodic components, the relative velocity $\mathbf{W}$ can be written as

$$\mathbf{W} = \bar{\mathbf{V}} - \omega \times \mathbf{r} + \mathbf{v} = \bar{\mathbf{W}}(r, z) + \mathbf{v}(r, \theta, z), \tag{6}$$

where $\mathbf{v}$ is the periodic component of velocity, $\bar{\mathbf{W}}$ is the circumferentially averaged component of

relative velocity, ω is the rotational velocity and $\mathbf{r}$ is the position vector. By neglecting the pitchwise variation in density, it is possible to show that the continuity equation of the mean flow is reduced to

$$\nabla \cdot \bar{\mathbf{W}} = -\bar{\mathbf{W}} \cdot \nabla \ln \bar{\rho}. \tag{7}$$

To account for blade blockage effects, a stream sheet thickness distribution can be included in this equation, namely

$$\nabla \cdot (\bar{\rho} B_f \bar{\mathbf{W}}) = 0, \tag{8}$$

where

$$B_f = 1 - \frac{t_\theta}{r} \frac{B}{2\pi}, \tag{9}$$

t_θ is the tangential thickness and r is the radius. The normal thickness (t_n) distribution obtained from stress considerations is used in conjunction with the estimated blade wrap angles to compute the tangential thickness from

$$t_\theta^2 = t_n^2 \left[1 + r^2 \left(\frac{\partial f}{\partial r} \right)^2 + r^2 \left(\frac{\partial f}{\partial z} \right)^2 \right]. \tag{10}$$

The continuity equation of the mean flow, equation (8), can be implicitly satisfied if we define a stream function Ψ, namely

$$\bar{V}_r = -\frac{1}{r B_f} \frac{\rho_i}{\bar{\rho}} \frac{\partial \Psi}{\partial z}, \qquad \bar{V}_z = \frac{1}{r B_f} \frac{\rho_i}{\bar{\rho}} \frac{\partial \Psi}{\partial r}, \tag{11}$$

where ρ_i is a reference density and Ψ is the so-called Stoke stream function for three-dimensional axisymmetric flow. To obtain an equation for the unknown stream function, let us consider the tangential component of the mean velocity,

$$\bar{\Omega}_\theta = \frac{\partial \bar{V}_r}{\partial z} - \frac{\partial \bar{V}_z}{\partial r}. \tag{12}$$

Now, if we substitute (4) for the LHS of equation (12) and use (11) to express the velocities in terms of the stream function, we can derive the following equation for the unknown stream function of the mean flow.

$$\frac{\partial^2 \Psi}{\partial r^2} - \frac{1}{r} \frac{\partial \Psi}{\partial r} + \frac{\partial^2 \Psi}{\partial z^2} + \frac{\partial \Psi}{\partial z} \left(\frac{\partial \ln(\rho_i/\bar{\rho})}{\partial z} + \frac{\partial \ln(1/B_f)}{\partial z} \right) + \frac{\partial \Psi}{\partial r} \left(\frac{\partial \ln(\rho_i/\bar{\rho})}{\partial r} + \frac{\partial \ln(1/B_f)}{\partial r} \right)$$
$$= -r B_f \frac{\bar{\rho}}{\rho_i} \left(\frac{\partial r \bar{V}_\theta}{\partial r} \frac{\partial f}{\partial z} - \frac{\partial r \bar{V}_\theta}{\partial z} \frac{\partial f}{\partial r} \right), \tag{13}$$

where the RHS is zero outside the blade region. This elliptic equation is solved subject to boundary conditions at the endwalls and upstream and downstream boundaries. The boundary condition at the endwalls (i.e. hub and shroud) is the no flow condition through these boundaries. This may be expressed as

$$\bar{\mathbf{V}} \cdot \mathbf{n} = 0,$$

where $\mathbf{n}$ is the unit vector perpendicular to the endwalls. This implies that the hub and shroud are the streamlines of the flow and so the Dirichlet boundary condition Ψ = constant applies at the endwalls.

The far upstream boundary condition is obtained from the known mean velocity far upstream (which is a design specification) by using

$$-\frac{1}{r}\frac{\rho_i}{\bar{\rho}}\frac{\partial \Psi}{\partial s}=\bar{\mathbf{V}}_{-\infty}\cdot\mathbf{n}, \tag{14}$$

where s is the distance along the far upstream boundary and $\mathbf{n}$ is the unit vector in the meridional plane normal to the far upstream boundary. In the absence of shed vorticity the velocity far downstream, $\bar{\mathbf{V}}_{\infty}$, will be uniform and hence the boundary condition is given by equation (14). By solving equation (13) subject to the above boundary conditions, the mean flow velocity field is determined.

For the calculation of the periodic flow let us consider the periodic component of vorticity, which is given by

$$\hat{\boldsymbol{\Omega}}=\boldsymbol{\Omega}-\bar{\boldsymbol{\Omega}}=(\nabla r\bar{V}_\theta\times\nabla\alpha)[\delta_p(\alpha)-1]. \tag{15}$$

However, Lighthill[17] has shown that

$$S'(\alpha)=\delta_p(\alpha)-1, \tag{16}$$

where $S'(\alpha)$ is the first derivative of the periodic sawtooth function $S(\alpha)$ with respect to α. The sawtooth function can be expressed in a Fourier series of the form

$$S(\alpha)=\mathrm{Re}\sum_{n=-\infty}^{\infty}\frac{e^{inB\alpha}}{inB}. \tag{17}$$

From equations (15) and (16) we obtain

$$\hat{\boldsymbol{\Omega}}=(\nabla r\bar{V}_\theta\times\nabla\alpha)S'(\alpha). \tag{18}$$

A Clebsch formulation for the periodic velocity which satisfies (18) is

$$\mathbf{v}(r,\theta,z)=\nabla\Phi(r,\theta,z)-S(\alpha)\nabla r\bar{V}_\theta, \tag{19}$$

where Φ is the potential function of the periodic flow. In the absence of circumferential variations in density the periodic component of the continuity equation can be written as

$$\nabla\cdot\mathbf{v}=-\mathbf{v}\cdot\nabla\ln\bar{\rho}. \tag{20}$$

Taking the divergence of (19) and using the continuity equation (20), we get

$$\nabla^2\Phi=S(\alpha)\nabla^2 r\bar{V}_\theta+(\nabla\alpha\cdot\nabla r\bar{V}_\theta)S'(\alpha)-\mathbf{v}\cdot\nabla\ln\bar{\rho}, \tag{21}$$

where the first two terms on the RHS will be zero outside the blade row. Since the flow is periodic in the pitchwise direction, we can express the potential function in terms of a Fourier series of the form

$$\Phi(r,\theta,z)=\sum_{n=-\infty}^{\infty}\Phi_n(r,z)\,e^{inB\theta}. \tag{22}$$

By expanding Φ and the RHS of equation (21) in terms of a Fourier series in the tangential direction, we can derive the following equation for the nth harmonic of the potential function of the periodic flow:

$$\frac{\partial^2\Phi_n}{\partial r^2}+\frac{1}{r}\frac{\partial\Phi_n}{\partial r}+\frac{\partial^2\Phi_n}{\partial z^2}+\frac{\partial\Phi_n}{\partial z}\frac{\partial\ln(\bar{\rho}/\rho_i)}{\partial z}+\frac{\partial\Phi_n}{\partial r}\frac{\partial\ln(\bar{\rho}/\rho_i)}{\partial r}-\frac{n^2B^2}{r^2}\Phi_n$$
$$=\frac{e^{-inBf(r,z)}}{inB}\left(\nabla^2 r\bar{V}_\theta+\frac{\partial r\bar{V}_\theta}{\partial r}\frac{\partial\ln(\bar{\rho}/\rho_i)}{\partial r}+\frac{\partial r\bar{V}_\theta}{\partial z}\frac{\partial\ln(\bar{\rho}/\rho_i)}{\partial z}\right)-e^{-inBf(r,z)}\left(\frac{\partial f}{\partial r}\frac{\partial r\bar{V}_\theta}{\partial r}+\frac{\partial f}{\partial z}\frac{\partial r\bar{V}_\theta}{\partial z}\right). \tag{23}$$

In order to solve (23) for the unknown Fourier coefficients of the potential function of the periodic flow, boundary conditions should be applied on the four boundaries of the physical domain. At the endwalls the periodic velocity normal to the hub and shroud must be zero. This condition can be expressed by

$$\mathbf{v}\cdot\mathbf{n}=0.$$

Substituting the Clebsch formulation for the periodic velocity (19) in the above expression, the following form of the wall boundary condition is obtained:

$$\frac{\partial\Phi_n}{\partial n}=\frac{\partial r\bar{V}_\theta}{\partial n}\frac{e^{-inBf(r,z)}}{inB}, \tag{24a}$$

where the partial derivatives are taken in the direction normal to the endwalls.

Far upstream and downstream the flow is uniform. This is the result of the fact that the periodic velocity dies away as the upstream boundary is approached. In the absence of shed vorticity the same phenomenon occurs as the far downstream boundary is approached. This condition can be implemented by imposing

$$\Phi_n=0. \tag{24b}$$

This implies zero tangential and axial components of periodic velocity far upstream and zero tangential and radial components of periodic velocity far downstream. Thus, for each of the harmonics n of the potential function of the periodic flow, equation (23) is solved subject to Neumann boundary conditions (24a) at the endwalls and Dirichlet boundary conditions (24b) far upstream and downstream.

The equations modelling the flow field have to be solved subject to the Kutta–Joukowski condition, i.e. the static pressure on the upper and lower surfaces of the blades must be equal at the trailing edge. The velocity jump across the blade has been shown by Tan *et al.*[12] and Borges[13] to be given by

$$\mathbf{W}^+-\mathbf{W}^-=\frac{2\pi}{B}\frac{(\nabla r\bar{V}_\theta\times\nabla\alpha)\times\nabla\alpha}{\nabla\alpha\cdot\nabla\alpha}. \tag{25}$$

The pressure (or enthalpy) jump across the blade can be determined from equation (25) by using the irrotational form of the inviscid energy equation (see Section 2.3). Thus it is possible to show that[16]

$$h^+-h^-=\frac{2\pi}{B}(\mathbf{W}_{bl}\cdot\nabla r\bar{V}_\theta), \tag{26}$$

where $\mathbf{W}_{bl}$ is the relative velocity at the blade. This simple expression offers a straightforward method of satisfying the Kutta condition by setting the RHS of (26) to zero so that

$$(\mathbf{W}_{bl}\cdot\nabla r\bar{V}_\theta)=0,$$

i.e. the gradient of $r\bar{V}_\theta$ along the meridional projection of the blade along the streamlines must be zero. This condition is *implicitly satisfied by specifying an $r\bar{V}_\theta$ distribution with zero meridional gradient at the trailing edge.*

2.2. Calculation of flow field—exact approach

In the previous subsection a description of the basic approach used for the computation of the mean and periodic flow fields was given. As a first approach the pitchwise variation of density was neglected and hence an approximate form of the continuity equation was used. The above approximate approach has the advantage that the density does not have to be computed

everywhere in the three-dimensional flow field. Although this mean density approach simplifies the numerical computation of the problem, it introduces errors in the computation of the flow field. In this subsection we shall present an approach for the solution of the mean and periodic flow fields when the exact forms of the continuity equations are used. The results of this exact approach will be used in Section 3 to investigate the effects of the mean density assumption on the accuracy of the method.

When the pitchwise variations in density are considered, the circumferentially averaged component of the continuity equation takes the form

$$\nabla \cdot \bar{\mathbf{W}} = -\overline{\mathbf{W} \cdot \nabla \ln \rho}. \tag{27}$$

Equation (27) cannot be used directly to define a stream function. Therefore we define a special mean density so that

$$\nabla \cdot \rho_m \bar{\mathbf{W}} = 0. \tag{28}$$

The value of ρ_m is determined by integrating the equation

$$\bar{\mathbf{W}} \cdot \nabla \ln \rho_m = \overline{\mathbf{W} \cdot \nabla \ln \rho}. \tag{29}$$

Then equation (28) can be used to define a stream function and, by using a procedure similar to that of the approximate approach, the governing equation of the mean flow can be derived.

In this case the periodic flow continuity equation is given by

$$\nabla \cdot \mathbf{v} = \overline{\mathbf{W} \cdot \nabla \ln \rho} - \mathbf{W} \cdot \nabla \ln \rho. \tag{30}$$

Thus equation (21) is modified to

$$\nabla^2 \Phi = S(\alpha) \nabla^2 r \bar{V}_\theta + (\nabla \alpha \cdot \nabla r \bar{V}_\theta) S'(\alpha) + \overline{\mathbf{W} \cdot \nabla \ln \rho} - \mathbf{W} \cdot \nabla \ln \rho. \tag{31}$$

Equation (31) is very similar to (21) apart from the third and fourth terms on the RHS, whose determination requires the computation of the velocity and density throughout the flow field. The problem is simplified a little by remembering that the flow is periodic in the tangential direction and hence the potential function may be expanded in terms of a Fourier series in that direction. For this purpose the Fourier coefficients of the third and fourth terms on the RHS of (31) have to be computed. However, since the differential equation is solved numerically, by using the finite difference approximations, the flow quantities are only known at discrete points inside the computational domain. Therefore numerical integration has to be used for the determination of the Fourier coefficients of these quantities. This is inaccurate, rather time-consuming and cumbersome.

Fortunately, there is a simple relationship between the Fourier transform of a function and its Fourier coefficients. Hence the discrete Fourier transform can be used to find the Fourier coefficients of the third and fourth terms on the RHS of (31). This has two advantages: firstly, there is no need for numerical integration; secondly, the discrete Fourier transform can be computed much more efficiently by using the fast Fourier transform algorithm.

The potential function may then be expressed in terms of an inverse discrete Fourier transform of the form

$$\Phi(r, \theta_j, z) = \sum_{n=-N/2}^{N/2-1} \Phi_n(r, z)\, e^{ik_n \theta_j}, \tag{32}$$

where $\theta_j = j\Delta\theta, j = 0, 1, 2, 3, \ldots, N$, gives the values of θ, the tangential co-ordinates of the points on a uniformly spaced grid in the tangential direction, with spacing $\Delta\theta$. The set k_n should be chosen to make the function $\exp(ik_n\theta_j)$ periodic and equally spaced and it should also reduce the

aliasing effects which can be found whenever a continuous function is sampled at discrete intervals. One such function is

$$k_n=\frac{2\pi n}{N\Delta\theta} \quad \text{for } n=-\frac{N}{2},\ldots,0,\ldots,\frac{N}{2}-1. \tag{33}$$

Thus by using equations (32) and (33) in equation (31), we get the following governing equation for the periodic flow:

$$\frac{\partial^2\Phi_n}{\partial r^2}+\frac{1}{r}\frac{\partial\Phi_n}{\partial r}+\frac{\partial^2\Phi_n}{\partial z^2}-\frac{n^2B^2}{r^2}\Phi_n=-R_n(r,z)+\frac{e^{-inBf(r,z)}}{inB}\nabla^2 r\bar{V}_\theta-\left(\frac{\partial f}{\partial r}\frac{\partial r\bar{V}_\theta}{\partial r}+\frac{\partial f}{\partial z}\frac{\partial r\bar{V}_\theta}{\partial z}\right)e^{-inBf(r,z)}, \tag{34}$$

when $n=-N/2,\ldots,-1,1,\ldots,N/2-1$ and

$$R_n(r,z)=\frac{1}{N}\sum_{j=1}^{N}(\mathbf{W}\cdot\nabla\ln\rho)e^{-i2\pi jn/N}. \tag{35}$$

The term obtained when n is equal to zero in equation (34) corresponds to the Clebsch formulation of the mean flow continuity equation and therefore has to be neglected in the solution of the periodic flow field. Since the potential function of periodic flow is a real function, its Fourier transform has the property $\Phi_{-n}=\Phi_n^*$, where $n=1, N/2$ and the asterisk denotes complex conjugation. As a result equation (35) is solved for one half of the frequency spectrum k_n given in equation (33) and subjected to the boundary conditions discussed in Section 2.1.

2.3. Calculation of density

The first law of thermodynamics applied to a steady flow process in the absence of viscous and body forces can be written as

$$\mathbf{W}\cdot\nabla H^*=0, \tag{36}$$

where $\mathbf{W}$ is the relative velocity vector and H^* is the rotary stagnation enthalpy or rothalpy. In the case of uniform flow at the inlet this equation reduces to

$$H^*=h+\tfrac{1}{2}(\mathbf{W}\cdot\mathbf{W})-\tfrac{1}{2}\omega^2r^2=\text{constant},$$

where ω is the rotational speed. By using the perfect gas equation and isentropic relations, it is possible to show that

$$\frac{\rho}{\rho^*}=\left(1+\frac{\omega^2r^2-(\mathbf{W}\cdot\mathbf{W})}{2C_pT^*}\right)^{1/(\gamma-1)} \tag{37}$$

In the case of the approximate approach the latest values of mean velocity, calculated from equation (11), are used in equation (37) to obtain a new estimate for the mean density. In the exact approach the full three-dimensional velocity field is used in (37) in order to obtain the density throughout the three-dimensional flow field. The mean velocity components are again obtained from equation (11), while the periodic velocities are computed by using the inverse Fourier transform and equation (19). For example, the radial component of the periodic velocity is computed from

$$v_r(r,\theta,z)=\text{IFT}\left(\frac{\partial\Phi_n(r,z)}{\partial r}-\frac{\partial r\bar{V}_\theta}{\partial r}\frac{e^{-ik_nf(r,z)}}{ik_n}\right), \tag{38}$$

where IFT represents the inverse Fourier transform. The following procedure is then used to find the RHS of the continuity equation, $\mathbf{W}\cdot\nabla\ln\rho$.

(i) The Fourier transform of the natural logarithm of the density ρ_n is computed.
(ii) The derivative of density in the tangential direction is then computed by taking the inverse Fourier transform of $(ik_n\rho_n/r)$, while the axial and radial derivatives of density are computed by calculating the inverse Fourier transform of the corresponding derivatives of ρ_n. Thus $\mathbf{W}\cdot\nabla\ln\rho$ is computed and then used in equation (35) to find R_n, which is required for the RHS of equation (34).

2.4. *Calculation of blade shape*

Once the flow field has been determined, it is then possible to compute the blade shape by using the blade boundary condition that the blade must be aligned to the velocity vector there. This condition can be expressed as

$$\mathbf{W}_{\mathrm{bl}}\cdot\nabla\alpha=0, \tag{39}$$

where $\nabla\alpha$ is a vector normal to the blade surface and $\mathbf{W}_{\mathrm{bl}}$ is the relative velocity at the blade surface ($\mathbf{W}_{\mathrm{bl}}=(\mathbf{W}^+ + \mathbf{W}^-)/2$, where $\mathbf{W}^+$ and $\mathbf{W}^-$ are the velocities on the upper and lower surface of the blades). Expanding (39),

$$(\bar{V}_z+v_{z\mathrm{bl}})\frac{\partial f}{\partial z}+(\bar{V}_r+v_{r\mathrm{bl}})\frac{\partial f}{\partial r}=\frac{r\bar{V}_\theta}{r^2}+\frac{v_{\theta\mathrm{bl}}}{r}-\omega, \tag{40}$$

where f is the wrap angle. Equation (40) is a first-order hyperbolic partial differential equation which has to be integrated along the meridional projections of streamlines on the blade surface in order to find the blade shape. The integration, as in the case of other initial value problems, cannot be completed without some initial condition on f. This initial value will be called the *stacking condition of the blade*. In this method the stacking condition is implemented by giving as input the values of blade wrap angle f along a quasi-orthogonal, for example at the leading edge.

2.5. *Numerical algorithm*

The partial differential equations for the computation of the flow field, i.e. equations (13), (23) and (34), and the blade shape, equation (40), are to be solved numerically by a finite difference approximation in the highly curved and complicated meridional geometry of radial and mixed flow machines, in which the boundaries are not coincident with the co-ordinate lines. As a result the implementation of the boundary condition will require interpolation between points nearest to the boundary, which can introduce unacceptable errors in the solution, particularly because the boundary conditions have a dominant influence on the character of the solution. To reduce this error, an algebraic transformation of co-ordinates from (r, z) to (ξ, η) was used, so that in the new curvilinear co-ordinate system the co-ordinate lines are coincident with the boundaries (i.e. hub and shroud coincide with lines of $\eta=$ constant and upstream and downstream boundaries correspond to lines of $\xi=$ constant); see Figure 1. More information on the transformation to the body-fitted co-ordinate system can be found in Reference 18. The form of the differential equations in the computational plane are presented in Appendix I.

The governing equations of the flow field in the computational plane, equations (46), (48) and (49), were discretized by using a second-order-accurate finite difference formula. The boundary conditions were then applied and the resulting simultaneous algebraic equations were solved iteratively, using Brandt[19] cycle C multigrid strategy to increase the rate of convergence. More

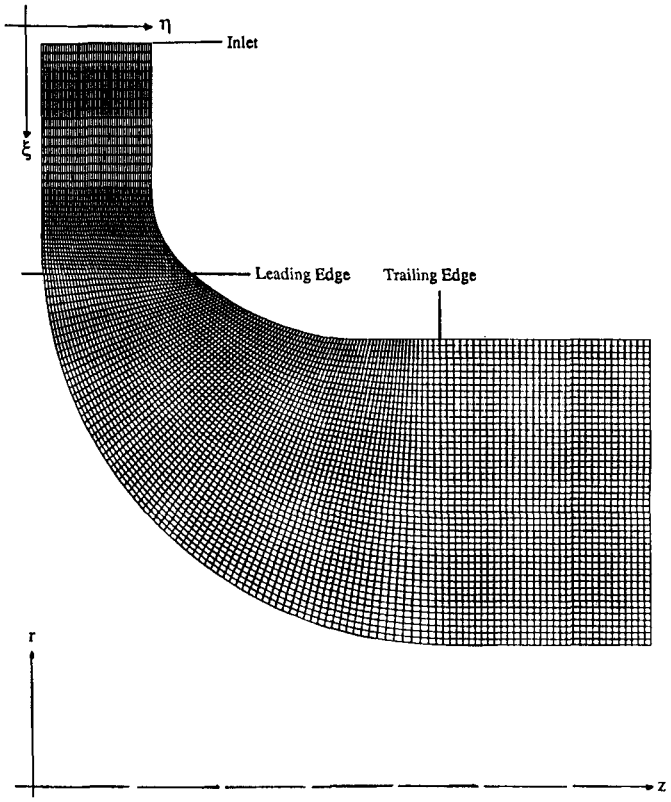

Figure 1. Computational mesh (145 × 49)

details on the discretization procedure and the form of the discretized equations can be found in Reference 16. The blade boundary condition, equation (50), and equation (29) for the determination of the special mean density ρ_m were discretized by using a scheme in which the partial differential equations are satisfied at the midpoints of the grid rather than at the grid points. This technique is sometimes referred to as the Crank–Nicholson method.[13,20]

To summarize, the following procedure is used for the iterative computation of the blade shape. First, the meridional geometry, design velocity triangles, inlet temperature, gas properties, stacking condition and $r\bar{V}_\theta$-distribution are specified. Then an initial guess for the blade shape is obtained from the specified $r\bar{V}_\theta$ and assuming uniform velocity. At this point the main iteration loop starts, in which the mean flow and then the periodic flow are computed. By using the mean velocities and the periodic velocities at the blade, the blade shape is determined and the above procedure is repeated until convergence is obtained. If the blade shape is computed without considering the periodic velocities, the resulting blade shape will correspond to the limiting case of an infinite number of blades or the so-called *actuator duct* (axisymmetric) solution.

2.6. Numerical difficulties

It was mentioned earlier that in the design method the blades are represented by sheets of vorticity. As a result the presence of the solid endwalls at the blades is modelled by the reflection of the vortex sheet (representing the blades) at the endwall. When the blades do not meet the

endwalls at right angles, the vortex system, consisting of the vortex sheet representing the blade and its reflection, results in a kinked vortex. This is illustrated in the diagram below, where AB is the vortex sheet representing the blade and AB′ is the reflection through the solid wall CD. BAB′ is the kinked vortex at the centre of which the induced velocity becomes infinite.

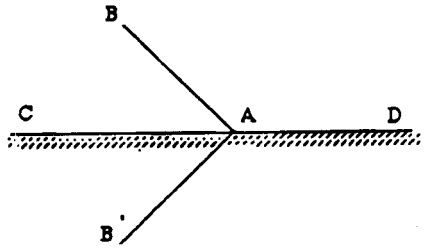

The presènce of this type of singularity was first reported by Kuchemann,[21] who investigated the flow at the junction of swept wings. This singularity has been found in the investigation of the flow in cascades of swept blades[11,22] and also in the analysis of flow through cascades of unswept blades with varying spanwise circulation.[23]

The presence of the singularity at the endwalls can also be interpreted as being due to the tangential component of bound vorticity which does not vanish at the walls. The bound vorticity in the present problem is given by equation (1). Therefore, to remove the singularity, we require that:

$$\bar{\Omega}_\theta = \frac{\partial r\bar{V}_\theta}{\partial n}\frac{\partial f}{\partial s} - \frac{\partial r\bar{V}_\theta}{\partial s}\frac{\partial f}{\partial n} = 0, \tag{41}$$

where n is normal and s is tangential to the endwalls. Now, Tan *et al.*[12] by considering the no flow condition at the endwalls have derived the following relationship:

$$\frac{\partial r\bar{V}_\theta}{\partial n} = \frac{\nabla\alpha\cdot\nabla r\bar{V}_\theta}{\nabla\alpha\cdot\nabla\alpha}\frac{\partial f}{\partial n}. \tag{42}$$

In general, $\nabla\alpha\cdot\nabla r\bar{V}_\theta \neq 0$, and if $\partial f/\partial n$ is continuous at the endwalls, then we can see from (42) that when $\partial r\bar{V}_\theta/\partial n$ is zero at the walls then $\partial f/\partial n$ must also be zero at the walls. This condition (first suggested by Smith[23]) forces the tangential component of the vorticity to vanish at the endwalls and thereby removes the singularity. However, in the present problem there are strong indications that $\partial f/\partial n$ is discontinuous. For example, the values of $\partial f/\partial n$ obtained from the code by Tan *et al.*[12] (who expanded f in the spanwise direction by using a cosine series) exhibited a clear Gibbs' phenomenon near the endwalls. Furthermore, the values of $\partial^2 f/\partial n^2$ seemed to show a delta function behaviour near the endwalls. Further investigations showed that it is possible to remove this singularity by putting both $\partial r\bar{V}_\theta/\partial n$ and $\partial f/\partial n$ to zero at the endwalls. As a result the endwall boundary condition (24a) for the potential function of the periodic flow is reduced to

$$\frac{\partial \Phi_n}{\partial n} = 0. \tag{43}$$

More detailed information on the nature of the endwall singularity can be found in Reference 16.

3. RESULTS

The three-dimensional inverse design method just described was applied to the design of a high (subsonic) speed radial-inflow turbine. The turbine was 135 mm in diameter and ran at a tip speed of 430 $m\,s^{-1}$ with a mass flow rate of 0·793 $kg\,s^{-1}$ and a design pressure ratio of 2·3. For the application of the method the meridional geometry was prescribed by a grid consisting of 145 quasi-orthogonals and 49 uniformly spaced quasi-streamlines. A plot of the grid used is shown in Figure 1; 35 quasi-orthogonals were used upstream of the blade and 77 quasi-orthogonals were used inside the blade region. In the Fourier expansion for the velocity 16 harmonics were considered.

The other inputs to the method were the distributions of $r\bar{V}_\theta$ and normal thickness throughout the entire meridional projection of the blade row. The normal thickness distribution was obtained after a few iterations between the inverse design programme and a three-dimensional structural analysis programme[16] to ensure the structural integrity of the impeller. The contours of specified $r\bar{V}_\theta$-distribution, non-dimensionalized by the blade tip speed and tip radius, are shown in Figure 2. The $r\bar{V}_\theta$-distribution was arrived at by specifying an optimum distribution on the hub

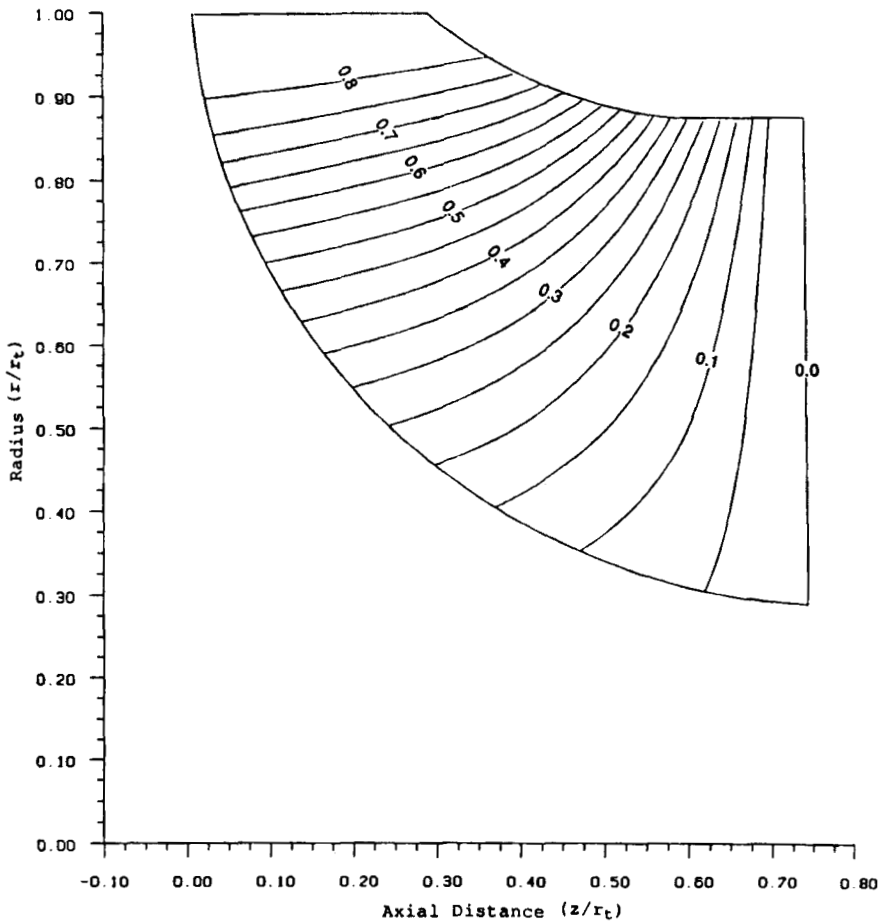

Figure 2. Contours of specified $r\bar{V}_\theta$-distribution

and shroud and then interpolating linearly between these two streamlines to find the overall $r\bar{V}_\theta$-distribution. In selecting the $r\bar{V}_\theta$-distribution, the following points were considered.

(i) The values of $r\bar{V}_\theta$ at the leading and trailing edges were obtained from the turbine's specific work. In the present example the value of $r\bar{V}_\theta$ was $0{\cdot}85 r_t U_t$ at the inlet and zero at the exit.

(ii) At the leading and trailing edges the derivatives of $r\bar{V}_\theta$ in the meridional direction were set to zero to satisfy the no-incidence and Kutta–Joukowsky conditions respectively (see equation (26)).

(iii) To eliminate the trailing vortex sheets and thereby reduce the exit kinetic energy loss, the same values of $r\bar{V}_\theta$ at the trailing edge were used across the span.

(iv) On the hub the distribution of $r\bar{V}_\theta$ between the leading and trailing edges was selected in such a way as to minimize the blade twist. The importance of this condition can be seen from the modified form of the blade boundary condition[16] used to calculate the blade shape:

$$\frac{\partial f}{\partial m} = \frac{\bar{V}_\theta - \omega r}{r V_m}. \tag{44}$$

In this equation f is the wrap angle, m denotes the meridional distance along the blades and all the periodic velocities have been neglected. From equation (44) it is possible to see that when the radius and meridional velocity are small (as on the hub streamline), the wrap angle can become unacceptably high. Therefore, to minimize the wrap angles, the relative tangential velocity should be kept to a minimum by specifying a $\bar{V}_\theta$-distribution that closely follows the blade speed.

(v) The shroud streamline is very highly loaded. Therefore, to suppress boundary layer separation, it is important to prescribe an $r\bar{V}_\theta$-distribution which gives a smooth pressure distribution on the shroud. Since by equation (26) the pressure (or Mach number) distribution is directly related to the derivative of $r\bar{V}_\theta$ in the meridional direction, care was taken to specify an $r\bar{V}_\theta$-distribution which has a smooth derivative. This can be seen by comparing Figure 3 with the Mach number distribution on the designed blade shown in Figure 5.

The above input data were then used in the design programme and the blade shape shown in Figure 4 was obtained. In this figure the blade shapes are presented along various axial (z = constant) planes, with the values of z at which the cuts were made shown on the plot. The value of $z = 0{\cdot}1$ mm corresponds to a point very near to the hub leading edge and the value $z = 48{\cdot}3$ mm corresponds to a line going through the trailing edge plane. From this figure it is possible to see that the computed blade shape is complicated with a double curvature near the tip. Obviously, it is very unlikely that this type of blade shape could have ever been designed by the iterative use of analysis or direct methods. The relative Mach number distributions on the designed blades are shown in Figure 5 and the contours of Mach number distribution on the suction surface are presented in Figure 6. By looking at Figure 5, we can see that a very smooth Mach number distribution has been obtained on the shroud.

In Section 2 we presented two different approaches for determining the flow field in compressible flow. The approximate (mean density) approach presented is more efficient computationally and in fact is about twice as fast as the exact method. However, the approximate method will introduce errors in the computation of the flow field and hence the blade shape. In this section we shall compare the results of the two methods for the high-speed radial-inflow turbine mentioned above.

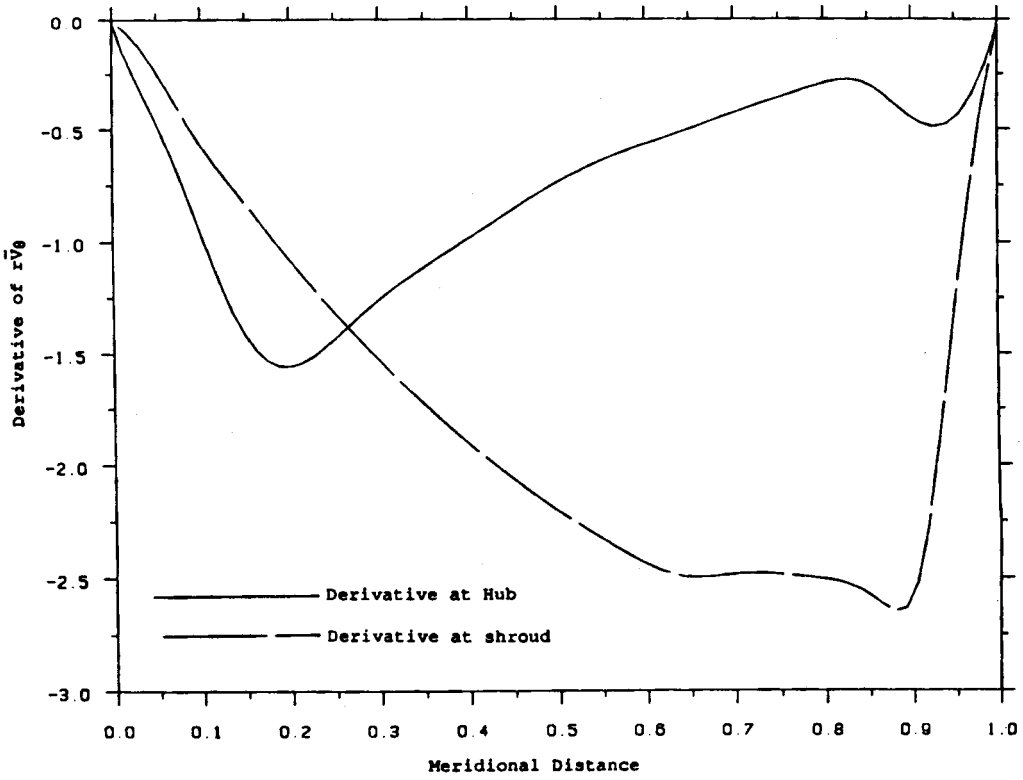

Figure 3. Meridional derivatives of $r\bar{V}_\theta$

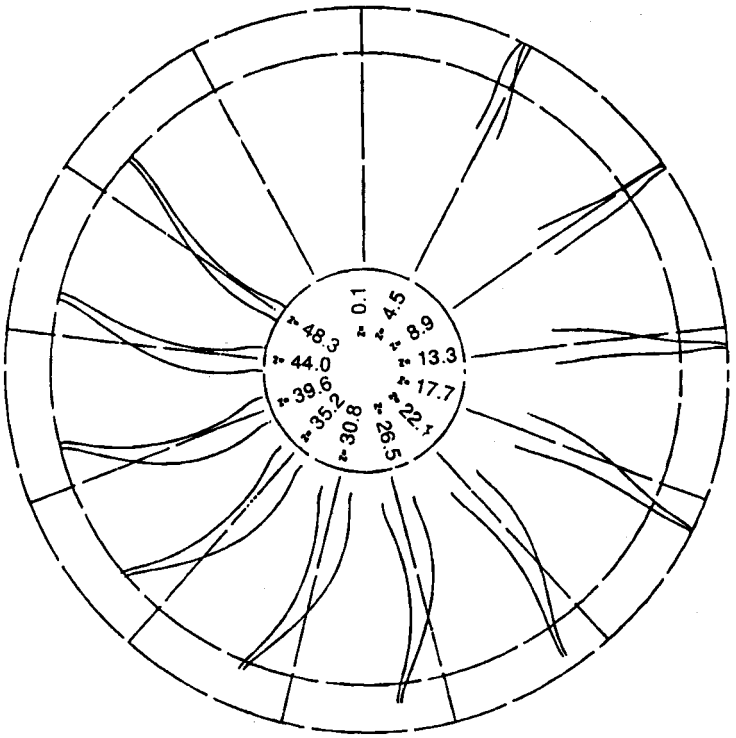

Figure 4. Axial sections of designed blade

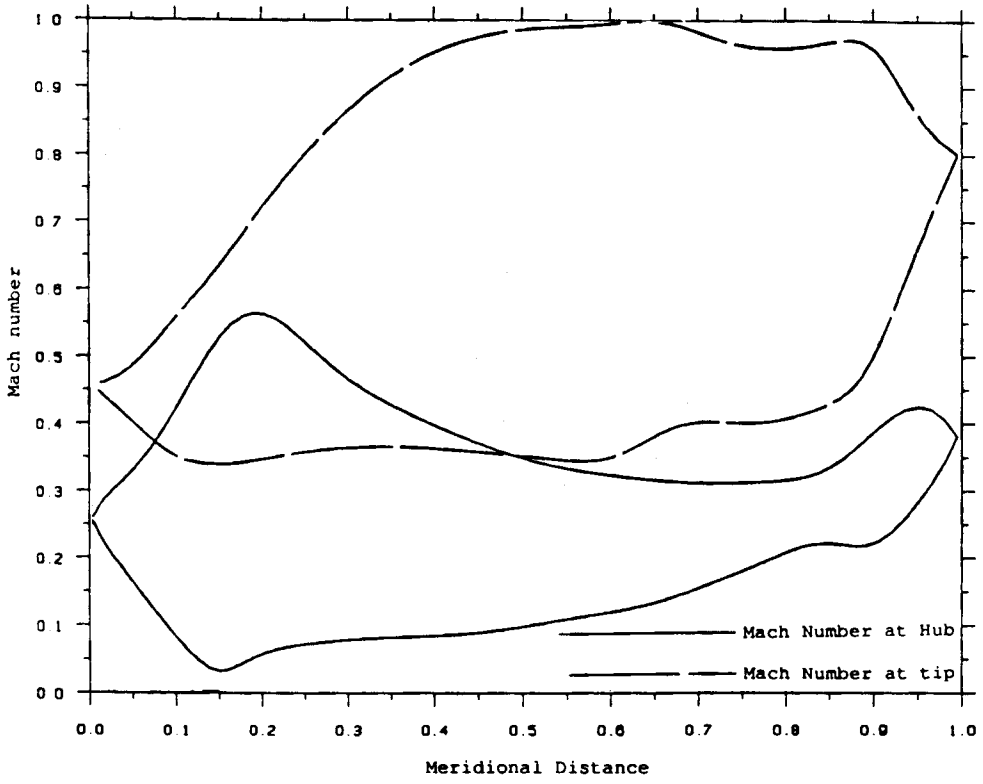

Figure 5. Surface Mach number distributions on designed impeller

To check the effect of the mean density assumption on the continuity equation, the divergence of mean relative velocity ($\nabla \cdot \bar{\mathbf{W}}$) is compared along the hub and shroud in Figures 7 and 8 respectively. The solid lines correspond to the values of $\nabla \cdot \bar{\mathbf{W}}$ obtained from the approximate continuity equation, i.e. $\bar{\mathbf{W}} \cdot \nabla \ln \bar{\rho}$. The dashed lines are the values of $\nabla \cdot \bar{\mathbf{W}}$ calculated from the exact form of the continuity equation of the mean flow, (27), and hence correspond to $\overline{\mathbf{W} \cdot \nabla \ln \rho}$. In Reference 24, expressions have been derived for the errors in the approximate continuity equation in terms of gradients of $r\bar{V}_\theta$ and the velocity at the blade. These expressions were derived by assuming linear pitchwise variation in density. The results shown in Figures 7 and 8 indicate that the expressions derived for the error terms can provide a good estimate of the magnitude of the errors.

The comparison of the relative Mach number on the hub and shroud is presented in Figure 9, where we can see that there is an appreciable difference between the Mach number distributions on the shroud, while the Mach number distributions on the hub are almost the same. Finally, the effect of the approximation on the blade shape is presented in Figure 10, where camber lines along five quasi-streamlines are compared. This plot shows that the approximation has little effect on the blade shape. In fact, the maximum absolute difference between the blade shapes is 0·00655 rad (0·37°), which is well within the manufacturing tolerance. Therefore we can conclude that the approximate (mean density) technique is capable of computing the blade shapes with a high degree of accuracy in subsonic flow.

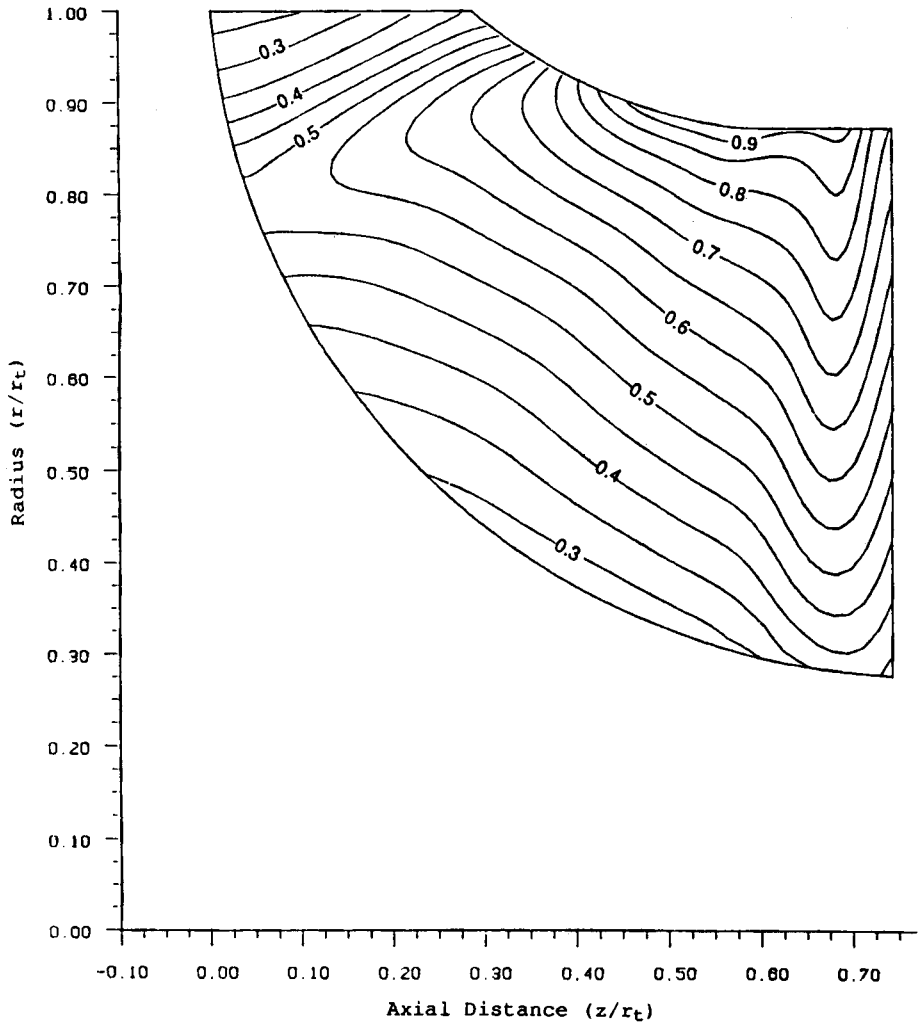

Figure 6. Contours of relative Mach number on suction surface by design method

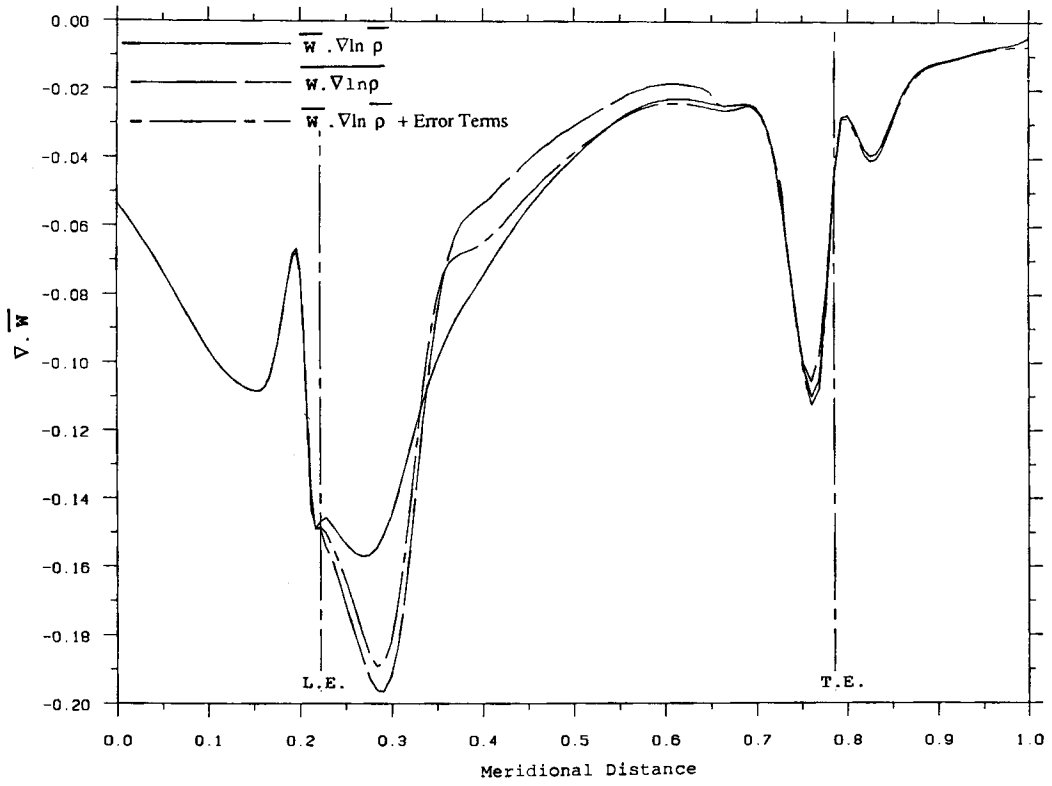

Figure 7. Comparison between approximate and exact approach divergence of mean relative velocity at hub

Finally, in order to check the accuracy of the design method and to close the loop consisting of the specification of $r\bar{V}_\theta$, the design method to compute the blade shape and the analysis of the flow through the designed impeller from which the $r\bar{V}_\theta$-distribution is computed, the flow through the designed impeller was computed by using Denton's[1] three-dimensional inviscid Euler solver. This method solves the finite volume form of the unsteady Euler equations of motion subject to steady boundary conditions by using a time-marching scheme to obtain the steady state solution.

The grid used for this calculation consisted of 59 quasi-orthogonals and 13 uniformly spaced streamwise and bladewise surfaces. From the computed relative tangential velocity the distribution of $r\bar{V}_\theta$ in the designed impeller was determined and its contours are shown in Figure 11. The computed contours of $r\bar{V}_\theta$ correlate very well to that prescribed, with the main difference occurring near the trailing edge where $r\bar{V}_\theta$ is negative rather than zero. At first, this small difference was attributed to two main causes: (i) the fact that the blade blockage was only approximately modelled and (ii) the use of the coarser grid in the time-marching analysis. To investigate the former, the blade was redesigned with zero thickness and then the flow through it was again computed by Denton's inviscid code. The computed distribution of $r\bar{V}_\theta$ for the

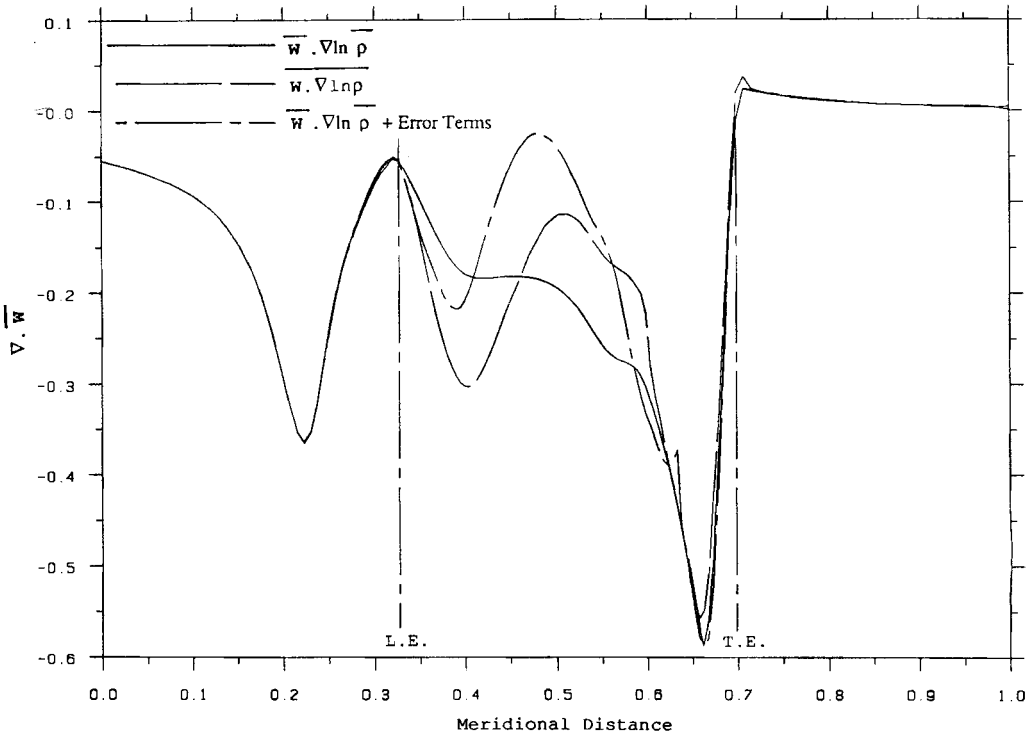

Figure 8. Comparison between approximate and exact approach divergence of mean relative velocity at shroud

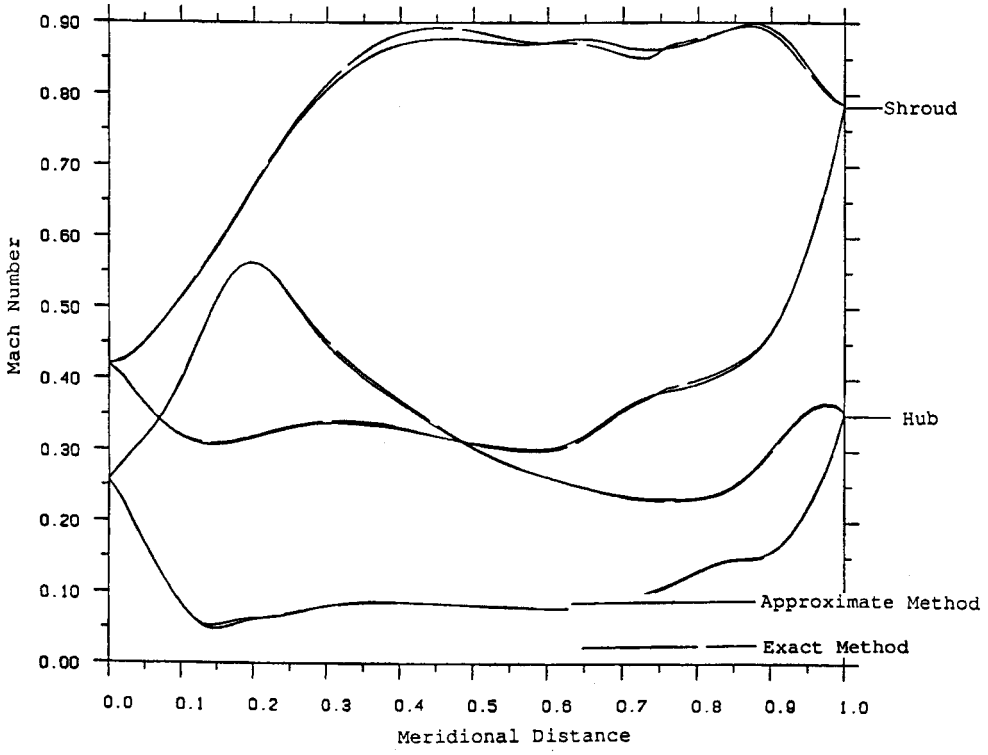

Figure 9. Comparison between approximate and exact approach surface Mach numbers

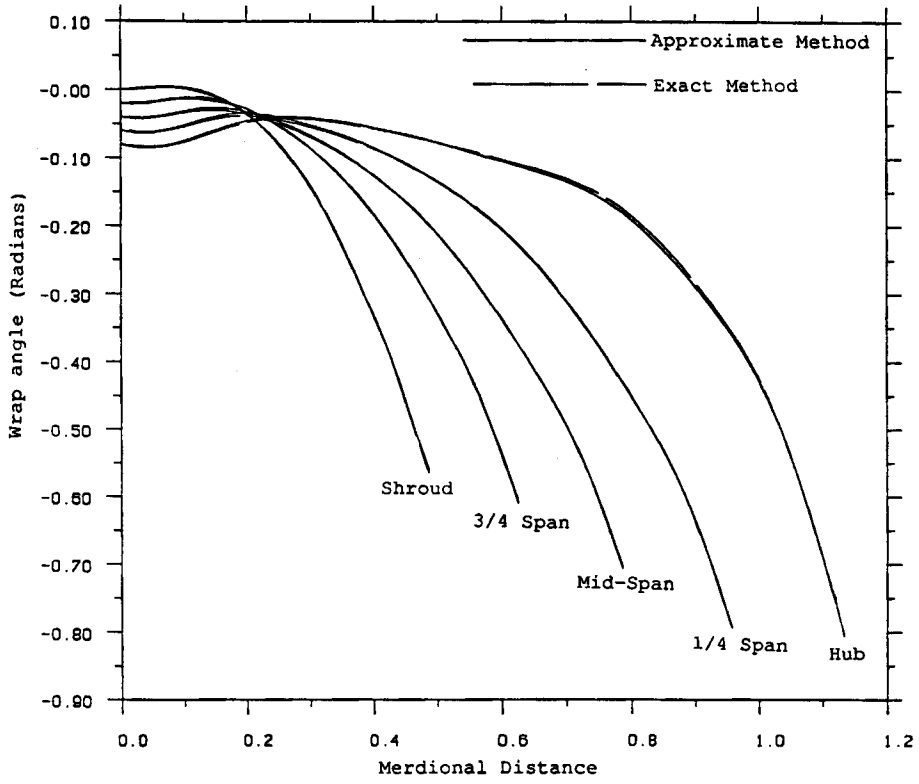

Figure 10. Comparison between approximate and exact approach blade shapes

zero-thickness design is presented in Figure 12. This is very similar to that computed for the original design, apart from a small difference near the leading edge. This is despite the fact that the blade shape obtained from the zero-thickness design is about 30% more twisted than that of the original design. Therefore we can make two important conclusions from these results: firstly, that the design programme can compute the blade shape with a very high degree of accuracy, and secondly, that the mean stream surface thickness parameter can, in subsonic flow, model the blockage effects quite accurately. As a result of further investigation we found that an appreciable amount of entropy (the value of $\exp(S/R)$ was as low as 0·93 near the trailing edge, while it should be 1·0 everywhere for a potential flow) was present in the time-marching solution, which must have been generated by artificial viscosity. Thus we can conclude with confidence that the difference in grid size is the main reason for the small discrepancy between the specified and computed $r\bar{V}_\theta$-distribution. The contours of relative Mach number on the suction surface of the blade computed by Denton's inviscid programme are shown in Figure 13. These also correlate very well with that predicted by the design programme.

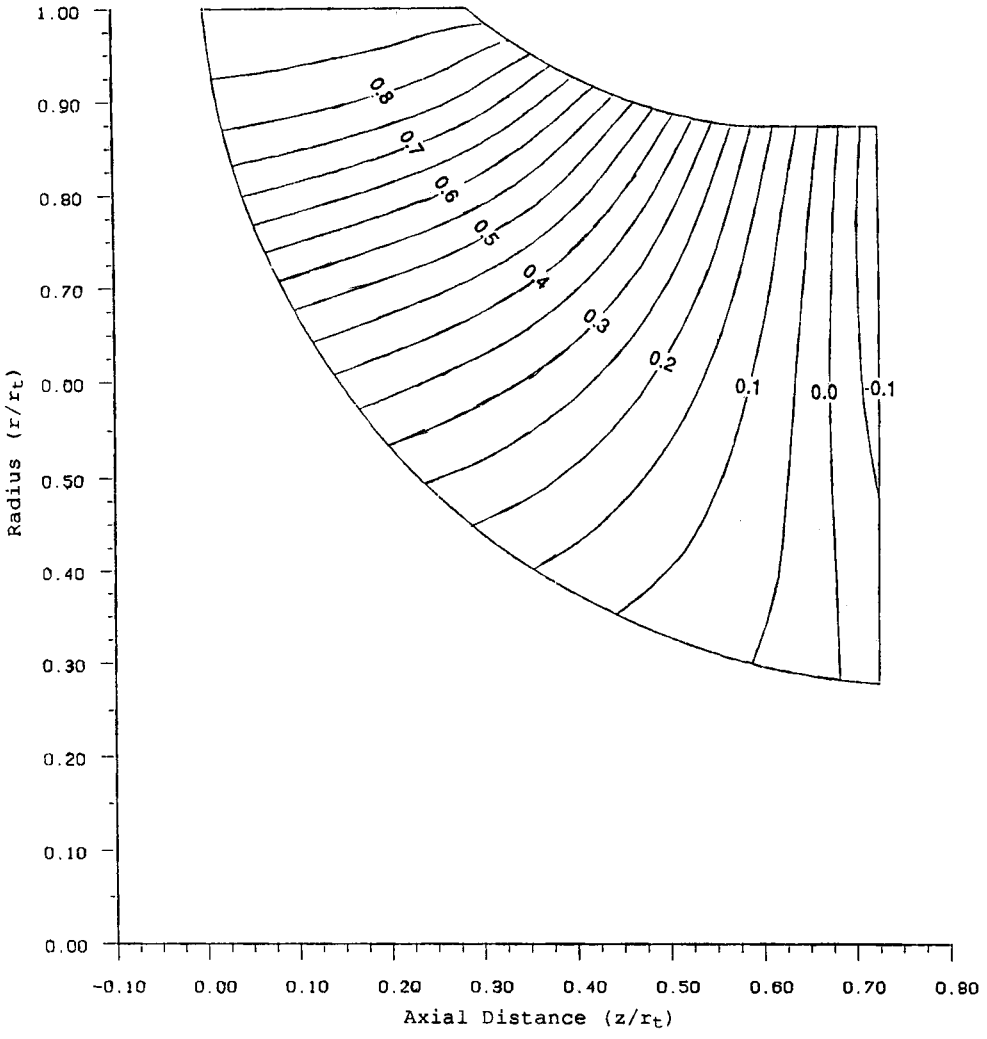

Figure 11. Contours of $r\bar{V}_\theta$ computed by inviscid Euler solver (with thickness)

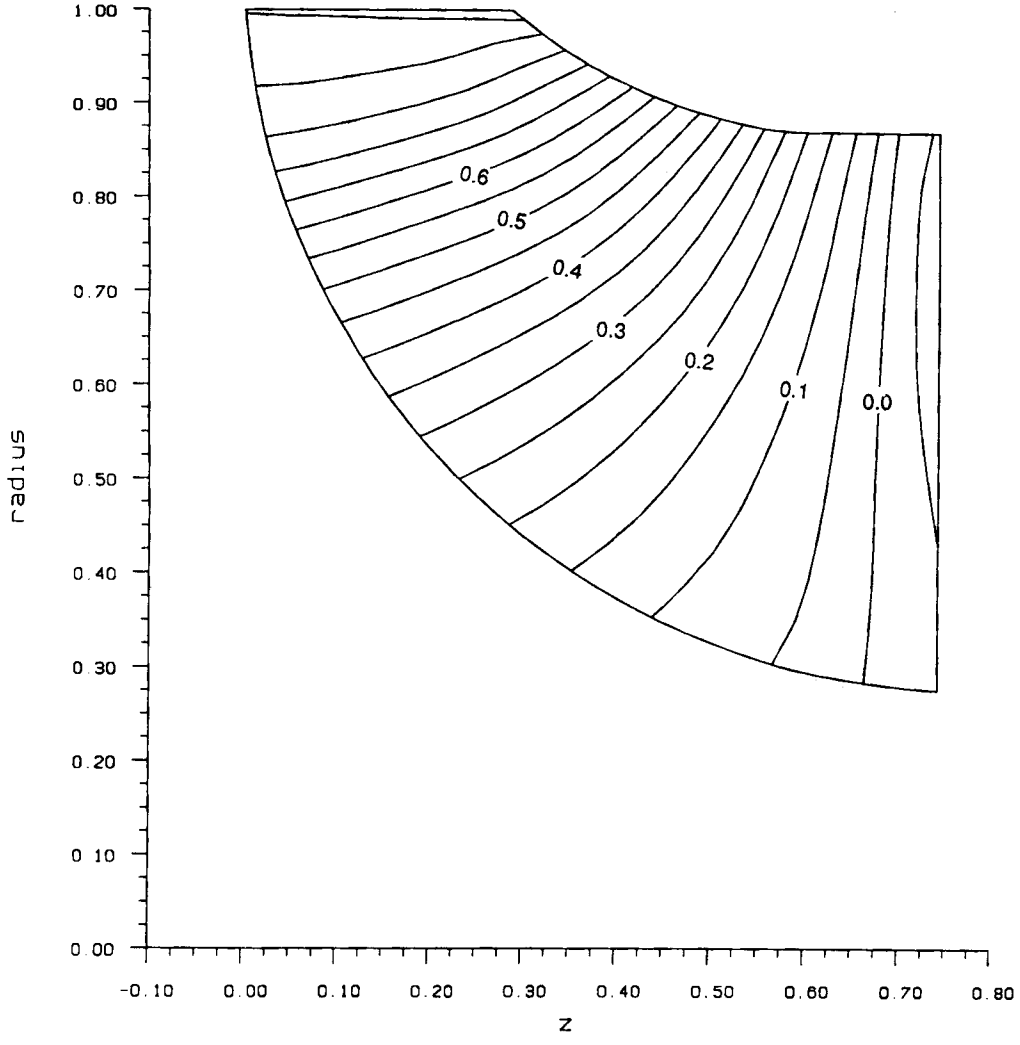

Figure 12. Contours of $r\bar{V}_\theta$ computed by inviscid Euler solver (zero thickness)

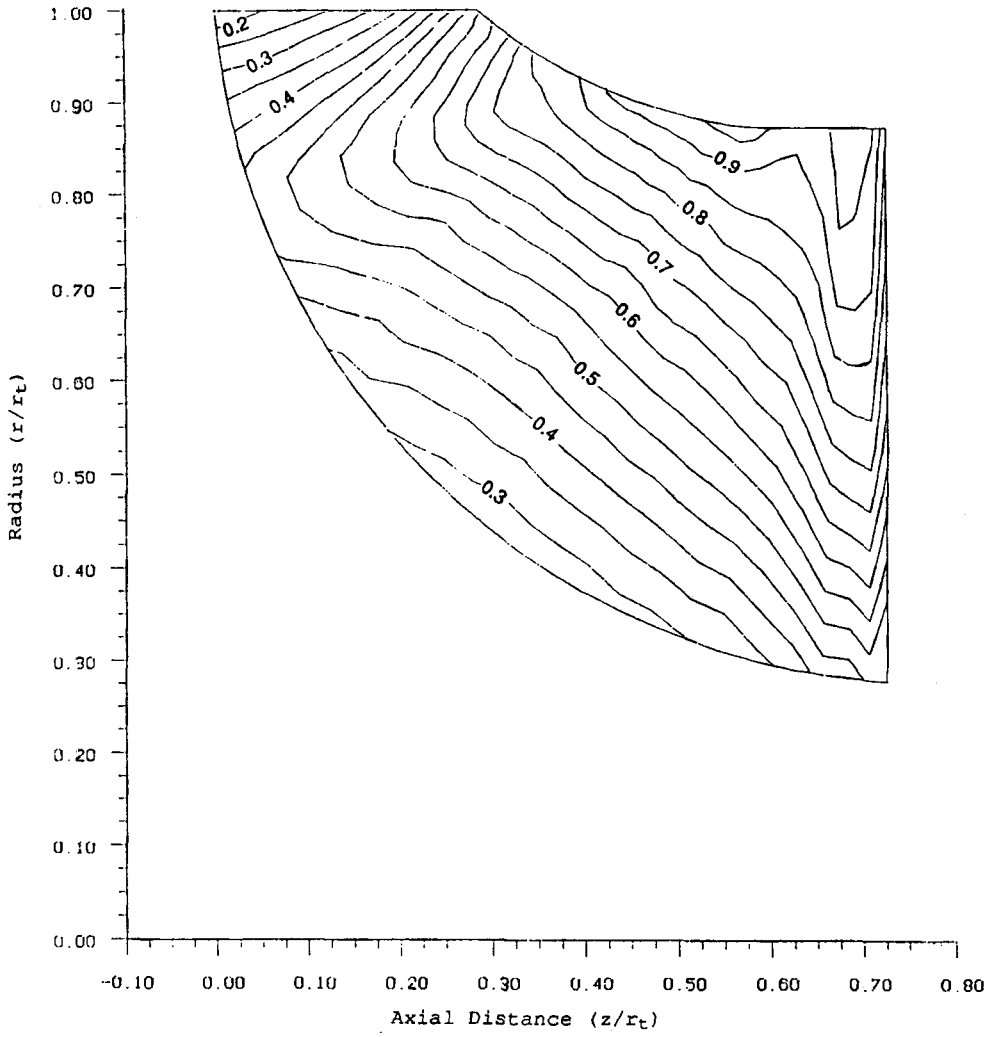

Figure 13. Contours of relative Mach number on suction surface computed by inviscid Euler solver

4. CONCLUSIONS

The development of a fully three-dimensional compressible inverse design method applicable to radial and mixed flow turbomachines has been described. The flow is assumed to be subsonic and inviscid and the blades are assumed to have negligible thickness, but blade blockage effects are approximately accounted for by using a mean stream surface thickness parameter in the continuity equation. Two approaches have been presented for solving the compressible flow problem. In the approximate approach the pitchwise variation in density is neglected and as a result the algorithm is simple and efficient. In the exact approach the velocities and density are computed throughout the three-dimensional flow field by employing a fast Fourier transform in the tangential direction. The results of the exact and approximate methods have been compared for the case of a high-speed radial-inflow turbine. It has been shown that the difference between

the blade shapes computed by the two methods is very small and well within the manufacturing tolerances.

To check the accuracy of the design method, the flow through the designed radial-inflow turbine was computed by using a three-dimensional inviscid Euler solver and the computed distributions of $r\bar{V}_\theta$ and Mach number were compared with that prescribed. Extremely good correlations were obtained, thereby validating the accuracy of the programme.

The method is currently being extended to transonic flows. The extension to transonic flows is important for high-pressure-ratio applications as well as in turbochargers, where as a result of the unsteady flow at the exhaust of the diesel engine, maximum turbine work is done at higher pressure ratios than those for which the turbines are presently designed.

ACKNOWLEDGEMENTS

This study was carried out while the author was a research student in the Whittle Laboratory of the University of Cambridge Engineering Department. The author would like to thank Professor Sir William Hawthorne for supervising this work and for his help and encouragement. During the course of this study the author was sponsored by Holset Turbochargers Ltd. of Huddersfield, U.K. and St. John's College, Cambridge. The author would like to thank both of these institutions which made the present study possible. The author is also grateful to the staff of the Whittle Laboratory for their comments and assistance. In particular, thanks are due to Dr. J. Borges who provided a plotting programme, to Dr. T. Hynes for his helpful comments and to Dr. J. D. Denton for his help in the use of his programme.

APPENDIX I

Once the grid in the physical domain has been generated, the relationship

$$\begin{bmatrix} r \\ z \end{bmatrix} = \begin{bmatrix} r(\xi, \eta) \\ z(\xi, \eta) \end{bmatrix} \tag{45}$$

between (r, z)-co-ordinates of the physical domain and (ξ, η)-co-ordinates of the computational domain is established. Then it can be shown that equation (13) takes the following form in the computational plane:

$$\begin{aligned} &\alpha\Psi_{\xi\xi} - 2\beta\Psi_{\xi\eta} + \gamma\Psi_{\eta\eta} + \Psi_\xi\left\{\tau + \frac{z_\eta J}{r} + \alpha\left[\left(\ln\frac{\rho_i}{\bar{\rho}}\right)_\xi + \left(\ln\frac{1}{B_f}\right)_\xi\right] - \beta\left[\left(\ln\frac{\rho_i}{\bar{\rho}}\right)_\eta + \left(\ln\frac{1}{B_f}\right)_\eta\right]\right\} \\ &\quad + \Psi_\eta\left\{\sigma + \frac{z_\xi J}{r} + \gamma\left[\left(\ln\frac{\rho_i}{\bar{\rho}}\right)_\eta + \left(\ln\frac{1}{B_f}\right)_\eta\right] - \beta\left[\left(\ln\frac{\rho_i}{\bar{\rho}}\right)_\xi + \left(\ln\frac{1}{B_f}\right)_\xi\right]\right\} \\ &\qquad = -rJ\frac{\bar{\rho}}{\rho_i}[f_\xi(r\bar{V}_\theta)_\eta - f_\eta(r\bar{V}_\theta)_\xi]. \end{aligned} \tag{46}$$

The transformation parameters in this equation are defined by

$$\begin{aligned} J &= z_\xi r_\eta - z_\eta r_\xi, & \alpha &= z_\eta^2 + r_\eta^2, \\ \beta &= z_\xi z_\eta + r r_\eta, & \gamma &= z_\xi^2 + r_\xi^2, \\ \tau &= \frac{z_\eta DR - r_\eta DZ}{J}, & \sigma &= \frac{r_\xi DZ - z_\xi DR}{J}, \\ DZ &= \alpha z_{\xi\xi} - 2\beta z_{\xi\eta} + \gamma z_{\eta\eta}, & DR &= \alpha r_{\xi\xi} - 2\beta r_{\xi\eta} + \gamma r_{\eta\eta}. \end{aligned} \tag{47}$$

Similarly, equation (23) takes the following form in the computational plane:

$$\alpha\Phi_{\eta\xi\xi}-2\beta\Phi_{n\xi\eta}+\gamma\Phi_{n\eta\eta}$$
$$+\Phi_{n\xi}\left[\tau-\frac{z_\eta J}{r}+\alpha\left(\ln\frac{\bar\rho}{\rho_i}\right)_\xi-\beta\left(\ln\frac{\bar\rho}{\rho_i}\right)_\eta\right]+\Phi_{n\eta}\left[\sigma+\frac{z_\xi J}{r}+\gamma\left(\ln\frac{\bar\rho}{\rho_i}\right)_\eta-\left(\ln\frac{\bar\rho}{\rho_i}\right)_\xi\right]-\frac{J^2n^2B^2}{r^2}\Phi_n$$
$$=\frac{e^{-inB_f(\xi,\eta)}}{inB}\left\{\nabla^2 r\bar V_\theta(\xi,\eta)+(r\bar V_\theta)_\xi\left[\alpha\left(\ln\frac{\bar\rho}{\rho_i}\right)_\xi-\beta\left(\ln\frac{\bar\rho}{\rho_i}\right)_\eta\right]-(r\bar V_\theta)_\eta\left[\gamma\left(\ln\frac{\bar\rho}{\rho_i}\right)_\eta-\beta\left(\ln\frac{\bar\rho}{\rho_i}\right)_\xi\right]\right\}$$
$$-e^{-inB_f(\xi,\eta)}\{f_\xi[\alpha(r\bar V_\theta)_\xi-\beta(r\bar V_\theta)_\eta]+f_\eta[\gamma(r\bar V_\theta)_\eta-\beta(r\bar V_\theta)_\xi]\}, \tag{48}$$

and equation (34) is transformed into

$$\alpha\Phi_{n\xi\xi}-2\beta\Phi_{n\xi\eta}+\gamma\Phi_{n\eta\eta}+\Phi_{n\xi}\left(\tau-\frac{z_\eta J}{r}\right)+\Phi_{n\eta}\left(\sigma+\frac{z_\xi J}{r}\right)-\frac{J^2n^2B^2}{r^2}\Phi_n$$
$$=-R_n+\frac{e^{-inB_f(\xi,\eta)}}{inB}\nabla^2 r\bar V_\theta(\xi,\eta)-e^{-inB_f(\xi,\eta)}\{f_\xi[\alpha(r\bar V_\theta)_\xi-\beta(r\bar V_\theta)_\eta]+f_\eta[\gamma(r\bar V_\theta)_\eta-\beta(r\bar V_\theta)_\xi]\}. \tag{49}$$

The blade boundary condition, equation (40), is transformed into

$$(\bar V_x+v_{\xi bl})f_\xi+(\bar V_\eta+v_{\eta bl})f_\eta=J^2\left(\frac{r\bar V_\theta}{r^2}+\frac{v_{\theta bl}}{r}-\omega\right), \tag{50}$$

where $v_{\xi bl}$, $v_{\eta bl}$ and $v_{\theta bl}$ are computed by using the following expressions:

$$v_{\xi bl}=\mathrm{Re}\sum_{n=-N/2}^{N/2-1}(\alpha\Phi_{n\xi}-\beta\Phi_{n\eta})e^{iknf(\xi,\eta)},$$
$$v_{\eta bl}=\mathrm{Re}\sum_{n=-N/2}^{N/2-1}(\gamma\Phi_{n\eta}-\beta\Phi_{n\xi})e^{iknf(\xi,\eta)}, \tag{51}$$
$$v_{\theta bl}=\mathrm{Re}\sum_{n=-N/2}^{N/2-1}\frac{nB}{r}\Phi_n e^{iknf(\xi,\eta)}.$$

APPENDIX II: NOMENCLATURE

B	number of blades
B_f	blockage factor (equation (9))
C_p	specific heat at constant pressure
$\hat{\mathbf{e}}$	unit vector
f	blade wrap angle (θ-value at the blade)
h	static enthalpy
r	radius
(r, θ, z)	cylindrical–polar co-ordinate system
$S(\alpha)$	sawtooth function
T	static temperature
$\mathbf{v}$	periodic velocity
$\mathbf{V}$	velocity
$\mathbf{W}$	relative velocity

α	angular co-ordinate of blade surfaces (equation (1))
$\delta_p(\alpha)$	periodic delta function
(ξ, η)	co-ordinates of the body-fitted curvilinear computational domain (Figure 1)
ρ	density
ρ_i	reference density
ρ_m	special mean density (equation (23))
Φ	potential function
Ψ	Stokes streamfunction (equation (12))
ω	rotational speed
$\mathbf{\Omega}$	vorticity

Subscripts

bl	at the blade
r	radial component
z	axial component (3D)
θ	tangential component

Superscripts

$\bar{(\ )}$	pitchwise mean value
$+$	relative to upper blade surface (facing positive θ); pressure surface in turbine
$-$	relative to lower blade surface (facing negative θ); suction surface in turbine
$\hat{(\ )}$	periodic quantities
$(\ )'$	differentiation w.r.t. argument

REFERENCES

1. J. D. Denton, 'An improved time marching method for turbomachinery flow calculations', *Trans. ASME, J. Eng. Power*, **105**, 514 (1983).
2. W. N. Dawes, 'Application of full Navier–Stokes solvers to turbomachinery flow problems', *VKI Lecture Series 2: Numerical Techniques for Viscous Flow Calculations in Turbomachinery Blading*, 1986.
3. C. Hah, A. C. Bryans, Z. Moussa and M. E. Tomsho, 'Application of viscous flow computations for the aerodynamic performance of a backswept impeller at various operating conditions', *ASME J. Turbomach.*, **110**, 303–311 (1988).
4. M. J. Lighthill, 'A new method of two-dimensional aerodynamic design', *ARC R&M 2104*, 1945.
5. R. I. Lewis, 'A method for inverse aerofoil and cascade design by surface vorticity', *ASME Paper 82-GT-157*, 1982.
6. G. Meauze, 'An inverse time-marching method for the definition of cascade geometry', *ASME J. Eng. Power*, **104**, 650–656 (1982).
7. M. Hart and D. S. Whitehead, 'A design method for 2D cascades of turbomachinery blades', *Int. j numer. methods fluids*, **7**, 1363–1381 (1987).
8. R. A. Novak and G. Haymann-Haber, 'A mixed-flow cascade passage design procedure based on a power series expansion', *ASME Paper 82-GT-121*, 1982.
9. X. Zhao, C. Sun and C. Wu, 'A simple method for solving three dimensional inverse problems of turbomachine flow and the annular constraint condition', *ASME Paper 84-GT-198*, 1984.
10. O. Ockuroumou and J. McCune, 'Lifting surface theory of axial compressor blade rows: Part I—Subsonic compressor, Part II—Transonic compressor', *AIAA J.*, **12**, (1974).
11. A. F. Falcao, 'Lifting-surface theory of straight cascades of swept blades', *Int. J. Mech. Sci.*, **18**, 313–320 (1976).
12. C. S. Tan, W. R. Hawthorne, C. Wang and J. E. McCune, 'Theory of blade design for large deflections: Part II—Annular cascades', *Trans. ASME, J. Eng. Gas Turb. Power*, **106**, 354–365 (1984); also *CUED/A-TURB/TR115*, 1982.
13. J. Borges, 'Three dimensional inverse design of turbomachinery', *Ph.D. Thesis*, Cambridge University Engineering Department, 1986.
14. W. S. Ghaly and C. S. Tan, 'A parametric study of radial turbomachinery blade design in three-dimensional subsonic flow', *ASME Paper 89-GT-84*, 1989.
15. W. R. Hawthorne, C. S. Tan, C. Wang and J. E. McCune, 'Theory of blade design for large deflections: Part I—Two dimensional cascades', *Trans. ASME, J. Eng. Gas Turb. Power*, **106**, 346–353 (1984).

16. M. Zangeneh, 'Three dimensional design of radial-inflow turbines', *Ph.D. Thesis*, Cambridge University Engineering Department, 1988.
17. M. J. Lighthill, *An Introduction to Fourier Analysis and Generalised Functions*, Cambridge University Press, Cambridge, 1967.
18. J. F. Thompson, F. C. Thames and C. W. Mastin, 'Boundary-fitted curvilinear coordinate systems for solution of partial differential equations on fields containing any number of arbitrary two dimensional bodies', *NASA CR-2729*, 1977.
19. A. Brandt, 'Multi-level adaptive solution to boundary value problems', *Math. Comput.*, **31**, 333–390 (1977).
20. P. J. Roache, *Computational Fluid Dynamics*, Hermosa, Albuquerque, NM, 1976.
21. D. Kuchemann, 'A simple method for calculating the span and chordwise loading on straight and swept wings for any given aspect ratio at subsonic speed', *ARC R&M 2935*, 1952.
22. L. H. Smith and H. Yeh, 'Sweep and dihedral effects in axial flow turbomachinery', *ASME J. Basic Eng.*, 401–408 (1963).
23. L. H. Smith, 'Secondary flow in axial flow turbomachines', *Trans. ASME*, **77**, 1065–1076 (1955).
24. M. Zangeneh, 'A compressible inverse design method based on an analytical approach', *CUED/A-TURB/TR125*, 1989.